Effects of Periodic Sequential Arrangement of Subscale Miura-Foldcore under Quasi-Static Compression

Chase Mortensen [a], Devin Nielsen [a], and S.Z.H. Shah [b], Juhyeong Lee [a, *]

[a] Department of Mechanical and Aerospace Engineering, Utah State University
[b] Department of Mechanical Engineering, Universiti Teknologi PETRONAS, Perak, Malaysia

[*]Corresponding author: juhyeong.lee@usu.edu

Abstract

This study presents experimental and numerical investigations on the quasi-static compressive responses of various subscale Miura-foldcore composites. A series of quasi-static compression tests were conducted on standard Miura foldcore specimens fabricated using carbon/epoxy woven fabric prepregs. Representative volume element (RVE) models, incorporating periodic boundary conditions (PBCs), were developed to predict the size-dependent compressive response of subscale Miura foldcores. The effective properties of the carbon/epoxy woven fabric composite used in this study were calculated using the NASA multiscale analysis tool (NASMAT) via two-step homogenization process. The FE model exhibited comparable agreement with experimental results, showcasing variations of less than 7% and 12% in maximum compressive load and compressive stiffness, respectively. The implementation of PBC in the foldcore RVE models improved modeling accuracy by <4%, but drastically increased total computational time (>50%). The periodic pattern of foldcore unit-cells, where two single foldcore unit-cells were placed in parallel or perpendicular, imposed geometric constraints, resulting in small variations in predicted stress and strain distribution contours. The key findings highlighted in this study suggest that a 1×1 foldcore unit-cell model without PBC is sufficient to predict accurate quasi-static compressive responses of foldcore composites. This study advances the understanding of subscale Miura-foldcore composites and provides valuable insights into the limitations associated with the use of PBC in foldcore RVE models. The findings also offer a

practical guide for fabricating and analyzing traditional Miura folding patterns, promoting a more efficient and accurate approach for optimizing foldcore composite designs considering both structural performance and manufacturability.

Keywords: Foldcore; Sandwich Structures; Quasi-Static Compression; NASMAT; RVE.

1 Introduction

Sandwich panels with conventional structural core materials (honeycombs, synthetic foams, balsa wood, etc.) are the primary composite structures found in advanced engineering applications [1,2]. Conventional structural cores have several drawbacks: (1) limited alteration of core geometric parameters, (2) limited core material selection, and (3) a closed-cell core network. *First*, deformation, failure modes, and structural performance of structure cores are strongly influenced by their geometric parameters (*i.e.*, pattern, wall-thickness, and height). Although honeycomb and polymer cores generally exhibit better mechanical properties, alteration of core geometric parameters is somewhat limited as it may require changes in the manufacturing process parameters. *Second*, it is known that honeycomb cores can be made of thin sheets of any material, but the two most commonly used core materials are aluminum and aramid paper. Although synthetic cores can be manufactured with any thermoplastics and thermosets with or without reinforcement, they have relatively low operating temperatures, weak structural performance, and environmental issues compared to legacy honeycomb core materials. Therefore, a few selected materials are recommended as structural polymer cores. *Lastly*, the closed-cell core network has a potential drawback of water/moisture being entrapped, resulting in significant mechanical property degradation [3]. Water/moisture ingress commonly occurs in conventional sandwich structures with considerable micro-cracks on their facings/skins, when aircraft cruise in moist high-altitude air, *i.e.*, upon descending at an altitude, moisture condenses and is trapped in the core [4]. In

addition, other fluid ingress contamination is a recurring problem that can cause performance degradation and reduced lifetime in sandwich structures.

These drawbacks can be overcome by using an origami-inspired foldcore with tunable geometric parameters and an open-cell core architecture [5–7]. Typical foldcores offer continuous fabrication and flexible core material selection, thus providing a dynamic tuning of structural performance [8,9]. Foldcores can be made of any thin metal sheets, carbon/glass/aramid/quartz fiber fabrics, and their hybrids [8]. Various structural applications and folding technologies have been developed in the past decades, proving the versatile and tailorable structural performance of foldcore sandwich composites (FSCs) [6,10,11]. Nearly non-limiting geometric parameters of foldcore can be designed to accommodate air and fluid flow, which makes it suitable for fluid transport applications, *i.e.*, heat exchangers and building ventilation systems [12].

Several quasi-static and dynamic mechanical tests and corresponding numerical simulations have been performed to understand the structural responses and associated damage modes of FSCs. Heimbs et al. [13] investigated FSCs with single and double-stacked foldcores under quasi-static compression and low-to-high velocity impact scenarios. Various geometric design variables (*i.e.*, a foldcore type, unit-cell geometry, core placement) were considered to optimize the shear rigidity and buckling/crushing resistance [14,15]. The transverse impact resistance and energy absorption of foldcore can be maximized by optimal foldcore design and appropriate material selection [16–18]. Numerical simulations are essential for assessing the performance of foldcore composite structures. Through numerical simulations, Miura foldcores with various folding patterns and materials have been investigated under different impact scenarios [10,19]. Numerical simulations, regardless of their fidelity and efficiency, have several major issues with imperfect implementation. Imperfections in the foldcore model are unavoidably

present in manufacturing, due to the foldcore's complex shape. Past research has introduced different techniques in finite element (FE) simulations [20,21].

In the last decades, numerous researchers have conducted parametric studies [22–27] to investigate static and dynamic mechanical properties influenced by core geometric parameters in various foldcores and their sandwich panels. Zhou et al. [22] conducted virtual testing on various single and multi-layered Miura foldcore composites under quasi-static compression, shear, and bending loading. The foldcores with curved fold lines showed better performance than the standard (flat) Miura foldcores in all loading conditions. The compressive and shear performance of multi-layered foldcores was found to be lower than that of single-layer foldcores, primarily attributed to the interaction between individual layers. Xiang et al. [23] conducted a comparable parametric investigation to understand the impact of core geometry and type on the quasi-static performance of Miura-foldcores, employing the plastic hinge theory. This study examined four fundamental geometric parameters of the core structure: parallelogram length, angle between parallelogram lengths, folding angle, and core thickness. The findings indicated that *i*) the peak compressive force remained unaffected by the side length*, ii*) a reduction in folding angle resulted in a decrease in the peak compression force along with an extended compressive force plateau, *iii*) the peak compressive force exhibited an increase as the parallelogram angle rose, reaching a maximum at 75°, and *iv*) a decrease in core thickness reduced the peak compressive force, while compressive stiffness remained unchanged. These findings aligned with the findings reported by Wang et al. [24]. The use of foldcores with lower areal density holds promise for enhancing structural integrity and collapsing force, but this may reduce the bending strength of the sandwich panel in comparison to a honeycomb core, as highlighted in a prior study [24]. Yuping et al. [25] reported that the parallelogram length and folding angle are the two most critical foldcore geometric parameters

affecting foldcore structural performance. Notably, an increase in folding angle can substantially improve the load-carrying capacity and energy-absorption characteristics of foldcore sandwich panels. Miura foldcores have numerous variations characterized by small geometric modifications. The indented foldcore, a variant of the standard Miura foldcore with small sub-folds along its top crease, demonstrated superior energy absorption performance with an improvement of up to 42%. In addition, an increase in the indentation angle decreased shear deformation [26]. As highlighted in various studies, improving the overall mechanical characteristics of Miura foldcores and their sandwich composite panels can be accomplished through the adjustment of key geometric parameters. In particular, rising folding angle [23,27], reducing parallelogram length [22,25,28,29], and increasing thickness [30–32] contribute to superior mechanical performance. Simultaneously modifying these geometric parameters significantly improves the performance of foldcore and associated sandwich panels [33].

A range of Miura foldcore variants, characterized by distinct curvature profiles, demonstrate superior performance compared to the standard Miura foldcore. Optimization of foldcore shapes also enhances the structural performance of sandwich panels. Foldcore geometric parameters and shapes can be optimized to improve the structural performance of sandwich panels. Ma et al. [34] introduced a novel kirigami-inspired pyramid foldcore sandwich panel and conducted a comprehensive comparison of its compression and shear resistance with that of conventional honeycomb core, standard Miura foldcore, and square egg-box core sandwich panels. This study [34] highlighted the potential for improved performance through the change of geometric configurations in foldcore design. The pyramid foldcore sandwich panel offered superior compression performance compared to honeycomb, Miura foldcore, and egg-box sandwich panels, with an average stress increase of 73%, 342%, and 130%, respectively.

Additionally, the shear resistance of the pyramid foldcore sandwich panel exhibited a 34% improvement when compared to the standard Miura foldcore sandwich panel. Hao et al. [35] introduced a virtual testing approach to predict the mechanical properties of various polyethylene terephthalate (PET) foldcores designed using the vertex method. This study involved a comprehensive analysis of the compression behaviors of standard Miura, zig-zag, and S-shaped Miura foldcores. Notably, the S-shaped Miura foldcore demonstrated the highest compressive force, showcasing a 10% improvement over the standard Miura foldcore. In the investigation conducted by Huang et al. [36], the structural performance of various cores, including two Miura foldcores (standard and curved-crease one), honeycomb, and birch continuous hexagonal (BCH) cores was examined. The findings indicated that curved-crease and BCH foldcores outperformed the standard Miura foldcore in both compression and shear loading. This underscores that the standard Miura foldcore as a baseline can be modified to enhance mechanical properties, depending on the loading direction. This observation aligns with the key conclusions in the previous studies [37–39]. Overall, the majority of Miura foldcores exhibited similar or improved (<20%) shear and bending performance, while showing slightly reduced compression performance compared to honeycomb cores [37]. For additional mechanical property improvement, the Resch foldcore, a Miura foldcore variant consisting of multiple polygon types was introduced for consideration [38]. Gattas et al. [39] reported that curved-crease foldcore was the only foldcore type exhibiting significant inertial strengthening under dynamic loading conditions. This provides an additional benefit for performance enhancement.

This paper focuses on determining the ideal specimen size for conducting quasi-static testing to validate FE models incorporating PBC implementation. Prior investigations have primarily focused on quasi-static mechanical testing on traditional Miura (or its variants) foldcores

made of metals or papers and the associated FE validation. These studies typically utilized component- or full-scale mechanical testing and FE model validation based on a simple RVE with PBC. Limited research has been conducted on both mechanical testing and FE simulations with and without PBC implementation for various subscale Miura foldcores subjected to quasi-static compression. Additionally, there has been a question regarding the necessity of PBC for achieving accurate FE simulations, given the significantly extended simulation time. This research aims to fill this gap in the existing literature by investigating the impact of RUC size and PBC on FE model accuracy. An in-depth understanding of the correlation between subscale mechanical testing and FE modeling associated with PBC can eliminate the necessity for conducting extensive testing. Through subscale analyses, we identify the optimal size for the Miura foldcore unit-cell specimen and whether PBCs must be maintained for accurate FE model prediction. This research focuses on the experimental and numerical characterization of the quasi-static compressive responses of three subscale carbon fiber reinforced polymeric (CFRP) Miura-foldcore specimens: (1) 1×1, (2) 1×2, and (3) 2×1 foldcores. Here, the 1×2 and 2×1 foldcores consist of two 1×1 foldcore unit-cells connected parallel and perpendicular, respectively. The technical background and key findings from this investigation are summarized in the following sections.

2 Technical Background

Figure 1 shows a baseline unit-cell model for standard Miura foldcore, defined as a type of origami-inspired folding pattern consisting of repeating tessellated shapes, with $\sigma^* = \sigma/\sigma_Y$ and $h^* = h/H$ each are dimensionless compressive stress and strain, where σ is the compressive stress, σ_Y is the compressive yield strength, h is the compressive displacement, and H is the initial height of the Miura foldcore specimen. As the Miura folding is still the most used pattern in foldcore composite studies, Gattas [16] researched various Miura foldcore variants, *i.e.*, indented

and curved-crease Miura foldcores. A curved-crease Miura foldcore increases the amount of energy absorption and ultimate compressive strength compared to the standard Miura foldcore.

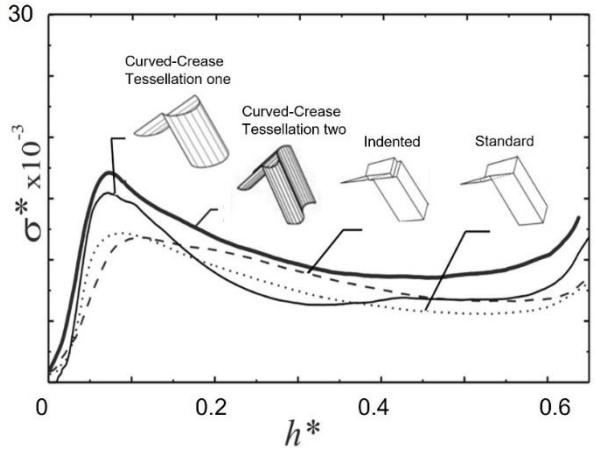

Figure 1. Compression performance for Miura foldcore variants: curved-crease tessellation one core, curved-crease tessellation two, indented, and standard cores [16]. σ^*represents the specimens' compressive stress divided by its compressive yield strength and h^* refers to the compressive displacement divided by the initial height of the foldcore specimen.

The foldcore geometric parameters used in this work were motivated by Heimbs et al. [10], as shown in Fig 2. Key core geometric parameters include height *H*, thickness *t*, cell length *L*, width *I*, and folding angle α. The mechanical properties of foldcore are strong functions of these geometric parameters. For instance, an increase in *I*, *H*, α, *t*, and a decrease in *L*, which in return an increase in an overall areal density, improves core compressive stiffness and maximum failure load [21]. Figure 3 shows typical compressive stress-strain curves of carbon/epoxy foldcore sandwich specimens prepared with different core geometries [40]. In the figure, Types B and C refer to two standard Miura foldcores with 0.48 mm and 0.50 mm thick carbon/epoxy layers, respectively. While both foldcores have the same height *H*, Type C has a greater thickness *t*, smaller length *L*, and a larger fold angle α, resulting in greater compressive fracture strength. The compressive stress linearly increases with increasing compressive strain and reaches a peak value of >6 MPa at the strain of ~1~2%. After fracture, the compressive stress drops rapidly with significant core cell crushing as the core walls meet the opposite skin. At higher compressions, the

specimen shows a gradual increase in the compressive strength in the densification regime due to material hardening.

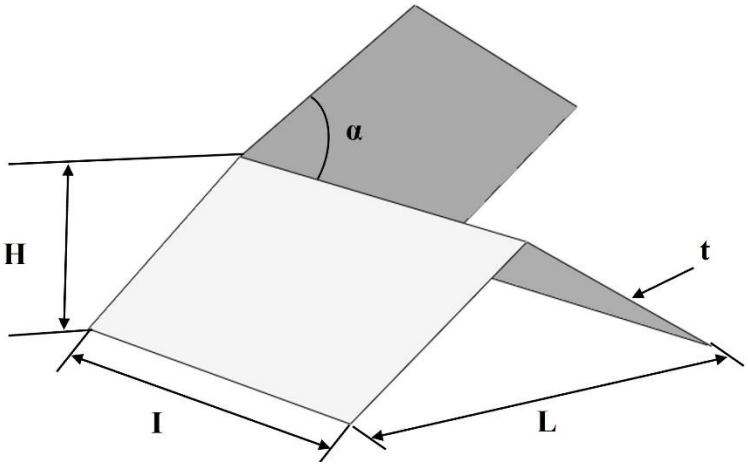

Figure 2. Foldcore unit-cell geometric parameters with core height *H*, core thickness *t*, cell length *L*, core width *I*, and fold angle *α*.

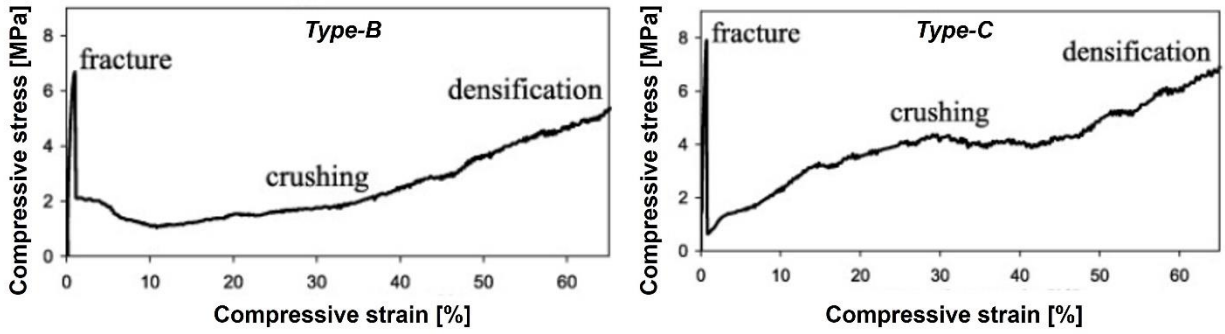

Figure 3. Normalized compressive stress-strain responses of two standard carbon/epoxy Miura foldcores: Type B (t = 0.48 mm, I = 29 mm, L = 10 mm, and $\alpha = 87°$) and Type C (t = 0.50 mm, I = 18 mm, L = 7.5 mm, and $\alpha = 118$) [40].

3 Foldcore Manufacturing

Miura foldcore specimens were manufactured with eight AS4/3501 carbon/epoxy woven fabric prepregs (HexForce™ AGP193-P carbon fabric (AS4 GP 3K yarns) pre-impregnated with HexPly® 3501-6 epoxy resin, Hexcel). Figure 4 shows a schematic of the CFRP foldcore manufacturing process used in this study. A discontinuous (batch) process was used to fabricate CFRP foldcores due to its easy-to-operate, uniform dimensions, and good overall part quality, compared to the resin transfer/resin infusion molding process. Both male and female molds were

machined out of 6061 aluminum alloy. The uncured, stacked laminate was placed between mating aluminum molds. For easy separation of panel and molds, perforated sheets were inserted between the prepreg and the mold. The laminate and mold were placed in a vacuum bag and cured using a 25-ton hydraulic heat press according to the manufacturer's recommendation (121°C for 1 hour followed by 2 hours at 177°C [41]). More details on in-house carbon/epoxy foldcore manufacturing process can be found in [42,43]. The cured 8-ply CFRP foldcores tested in this work dimensioned 140 × 140 × 16 mm^3 and had a nominal thickness of 1.6 mm. All foldcore specimens were manufactured from a single mold to maintain uniform specimen quality. This can minimize specimen-to-specimen variations associated with different batch processes.

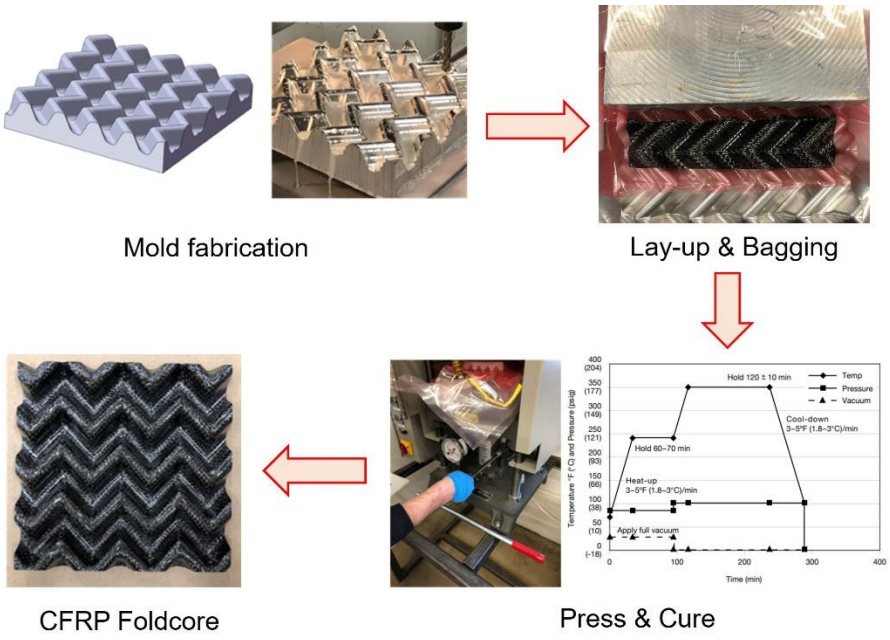

Figure 4. Manufacturing process of 8-ply carbon/epoxy foldcore.

The cured foldcore was cut into three subscale unit-cell specimens using a circular wet saw with a diamond-coated blade: (1) 1×1, (2) 1×2, and (3) 2×1. The final dimensions of a baseline 1×1 foldcore specimen were approximately 40 mm × 33 mm × 16 mm. The 1×2 and 2×1 foldcore specimens defined herein refer to those, where two baseline foldcore unit-cells are connected *parallel* and *perpendicular*, respectively. Figure 5 shows a schematic of a baseline foldcore

specimen along with its dimensions. Three different foldcore unit-cell specimens were prepared for quasi-static mechanical testing. Due to the complex foldcore geometry, orthotropic nature of woven fabrics, and non-uniform temperature and pressure distributions during cure, the foldcore specimens showed small variations in thickness ranging from 1.4-1.5 mm. For instance, the 1×1 and 1×2 specimens had a nominal thickness of ~1.4 mm, and the 2×1 specimens showed a nominal thickness of ~1.5 mm. Note that this variation in foldcore specimen thickness results from non-uniform temperature and pressure distributions within the mold associated with complex core geometry. A batch-to-batch variation in foldcore specimen dimension was negligible (≪ 0.1 mm). A detailed description of the foldcore manufacturing process is provided in our previously published study [44].

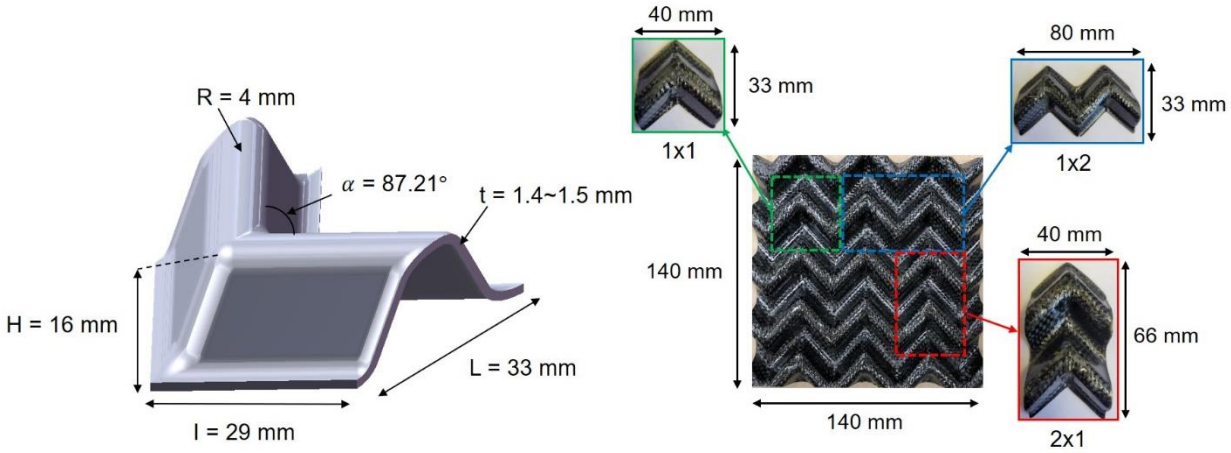

Figure 5. Foldcore unit-cell specimens used for mechanical testing.

4 Quasi-Static Compression Testing

A series of quasi-static compression tests were performed on foldcore specimens according to ASTM C365 [45], using an MTS Bionix servo-hydraulic testing frame equipped with a 25 kN load cell. The displacement rate was 3 mm/min. At least four specimens were tested for each foldcore unit-cell configuration to obtain statistically reliable results. In this work, the compression

was terminated when the specimen reached a displacement of 8 mm. Figure 6 shows a baseline 1×1 foldcore specimen positioned at the center between two compression platens.

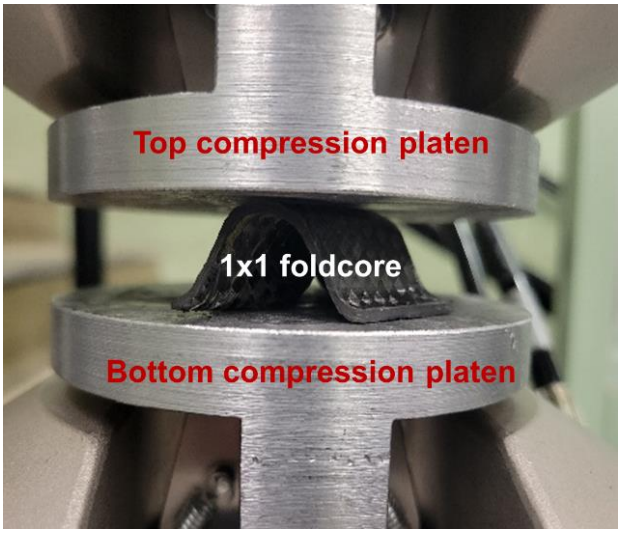

Figure 6. Quasi-static compression testing setup for 1×1 foldcore specimen.

Figure 7 shows the deformation and damage evolution of a representative 2×1 foldcore unit-cell specimen. Although not included herein, similar damage progression was seen in the other foldcore unit-cell specimens. After 3 mm of compressive displacement (at $t = 1$ min), core crushing occurred at the peak region of the core. Note that the core dimensions are slightly different due to complex foldcore geometry, orthotropic woven fabric properties, and non-uniform temperature and pressure distributions during cure; thus, the evolution of core crushing was not uniform. Around 6 mm of compressive displacement ($t = 2$ min), core crushing was observed in another peak region, along with severe ply separation at the crushed core. At the termination of the compression test ($t = 2.5$ min), all core peak regions showed considerable delamination.

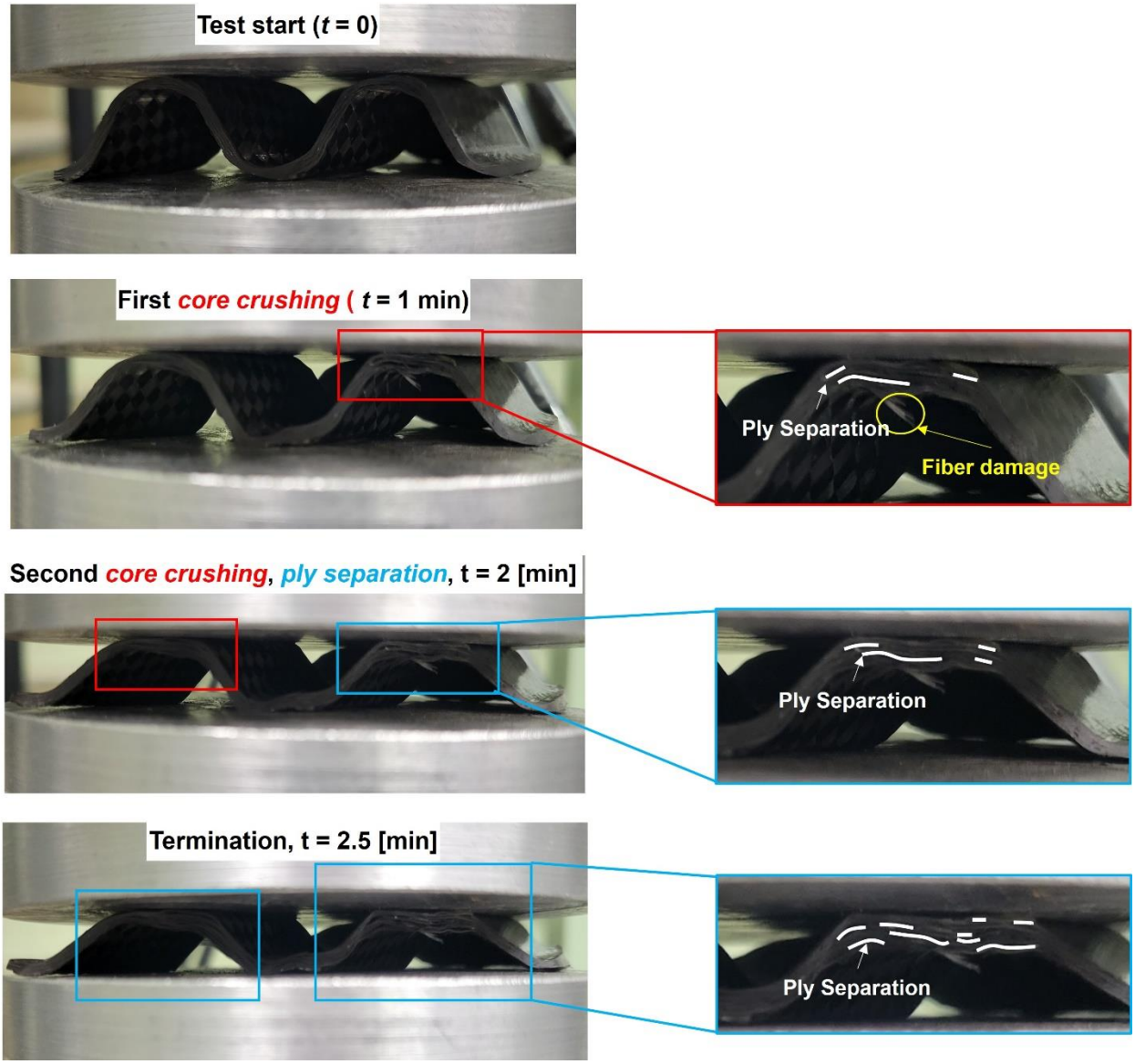

Figure 7. Deformation and damage evolution of a 2×1 unit-cell specimen. In the figure, red and blue dotted boxes indicate the regions with core crushing and ply separation, respectively.

5 Finite Element Model

5.1 Effective Property Calculation

The NASA's multiscale analysis tool (NASMAT) [46] is an integrated recursive framework for a multiscale and multi-fidelity modeling tool developed at the NASA Glenn Research Center (GRC). NASMAT is based on multiscale recursive micromechanics (MsRM) theory to deploy a variety of micromechanics formulations on an arbitrary number of hierarchical scales within a

structure. NASMAT can determine homogenized material properties of heterogeneous composite from its constituents (*i.e.*, fiber, matrix, and interface) [46]. In this work, the effective elastic properties, and strengths of carbon/epoxy woven fabric composites were calculated using the generalized method of cells (GMC) micromechanics theory as supported by NASMAT. This calculation was necessitated by the absence of mechanical property data for our composites. Indeed, a micromechanics framework facilitates the accurate prediction of effective properties, characterizing the physical microstructure of composites. While NASMAT proves to be powerful for analyzing composite materials in a multiscale-recursive framework, the present study focused on determining effective material properties. Directly integrating a NASMAT micromechanical model into a FE model requires proprietary application program interfaces (APIs), such as FEAMAC. Table 1 summarizes room temperature properties for the AS4 carbon fiber and the 8552-epoxy matrix used in the NASMAT simulation [41,47]. Note that the shear strength of the HexPly® 3501-6 epoxy matrix was not available in open literature: 3506-1 and 8552 epoxy matrix systems have similar room temperature properties. Therefore, we have used 8552 epoxy matrix properties in the NASMAT model.

Table 1. AS4 carbon fiber and 8552 epoxy material properties used in the NASMAT model.

Description	**Symbol**	**AS4 Fiber** [41]	**8552 Epoxy** [47]
Longitudinal Modulus [GPa]	E_{11}	225	4.2
Transverse Modulus [GPa]	E_{22}	15	4.2
Poisson's Ratio	v_{12}	0.2	0.34
Shear Moduli in 1-2 plane [GPa]	$G_{12} = G_{13}$	15	1.56
Axial Tensile Strength [MPa]	S_{11}	4480	45
Transverse Tensile Strength [MPa]	$S_{22} = S_{33}$	81	45
Shear Strength [MPa]	S_{23}	64	48.3

For effective property calculation, NASMAT analysis was performed with a standard linear elastic model for each constituent, assuming perfect fiber-matrix bonding; no interface was considered. Figure 8 shows a schematic of the general method of cell (GMC) discretization for the plain weave composite as part of a two-step multiscale homogenization. In step-1 (tow homogenization), each fiber tow was discretized using the square pack fiber-matrix geometry. In step-2 (plain weave homogenization), a plain-woven fabric was modeled. In the plain weave, each warp yarn passes over and then under the weft yarns, thus tow stacking sequences are locally varying. This is shown in Fig. 8, where the color in each subcell/subvolume indicates different tow stacking sequences. The fiber undulation was only considered in the regions between the fiber overlap regions in step-2 homogenization where it was approximated as a constant angle. In the figure, the grey subcells refer to fiber tow subcells with homogenized properties from step-1. The dark and light grey shades indicate cases where tows are primarily oriented in the 3- and 2-directions respectively. The white subcells indicate pure matrix regions. The in-plane and out-of-plane tensile strengths of the plain weave RUC were calculated in NASMAT using maximum stress criteria.

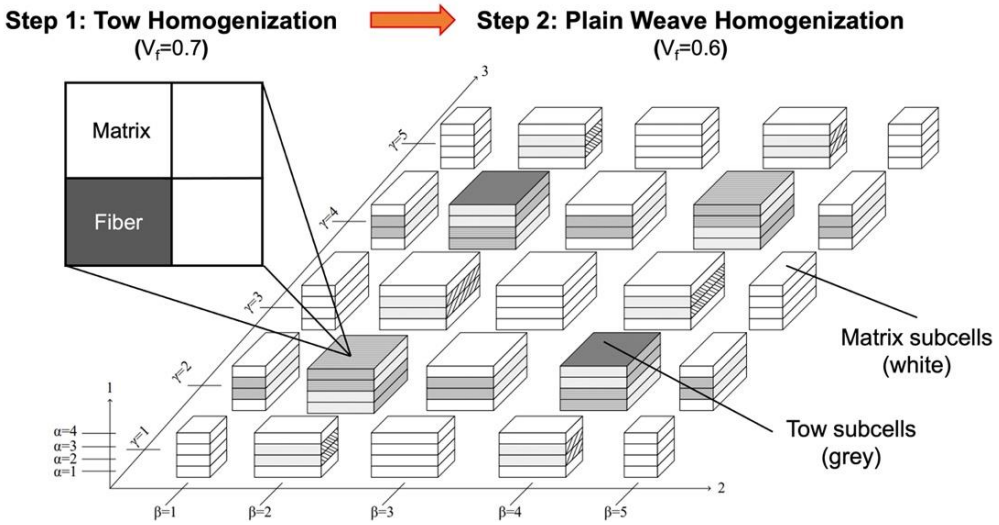

Figure 8. Two-step homogenization of the plain weave composite in NASMAT [46].

Table 2 includes homogenized AS4/8552 woven fabric properties predicted from NASMAT with a tow fiber volume ratio of 0.7 (step-1, tow homogenization), an overall fiber volume fraction of 0.6 (step-2, plain weave homogenization), and an out-of-plane fiber distortion angle of 14.03° from the overlap between the fibers in the plain weave. This angle is consistent with the out-of-plane distortion of plain-woven fabric [48]. In this work, NASMAT determined homogenized longitudinal and transverse moduli, shear moduli, tensile strengths, shear strength, and Poisson's ratio of the AS4/8552 carbon/epoxy woven composite, while fracture energies and compressive strengths used for further analysis were obtained from the literature [49].

Table 2. AS4/8552 carbon/epoxy material properties used in the FE models.

Description	Symbol	Value	Comment
In-Plane Modulus [GPa]	E_{11}	61.45	NASMAT
Out-of-Plane Modulus [GPa]	E_{22}	10.35	
Poisson's Ratio	ν_{12}	0.054	
Shear Moduli in 1-2 plane [GPa]	$G_{12} = G_{13}$	3.52	
Shear Moduli in 2-3 plane [GPa]	G_{23}	2.5	
In-Plane Tensile Strength [MPa]	X_T	133	
Out-of-Plane Tensile Strength [MPa]	Y_T	60	
In-Plane Shear Strength [MPa]	S	40.7	
Longitudinal tensile fracture energy [kJ/m^2]	G_{1f+}	50	[49]
Longitudinal tensile compressive energy [kJ/m^2]	G_{1f-}	72	
Transverse tensile fracture energy [kJ/m^2]	G_{2f+}	47	
Transverse compressive energy [kJ/m^2]	G_{2f-}	67	
In-Plane Compressive Strength [MPa]	X_C	862	[41]
Out-of-Plane Compressive Strength [MPa]	Y_C	388	

5.2 Damage Laws

The two-dimensional (2D) Hashin damage (initiation) criteria, available in ABAQUS [50,51], were used to estimate fiber and matrix damage in all foldcore unit-cell models. The Hashin

criteria provide four distinct damage modes: fiber failure in tension (Eqn. 1), fiber failure in compression (Eqn. 2), matrix failure in tension (Eqn. 3), and matrix failure in compression (Eqn. 4). Damage initiates when the following criteria are met:

$$F_t = \left(\frac{\sigma_{11}}{X_T}\right)^2 + \beta\left(\frac{\tau_{12}}{S_{12}}\right)^2 \geq 1 \quad (1)$$

$$F_c = \left(\frac{\sigma_{11}}{X_C}\right)^2 \geq 1 \quad (2)$$

$$M_t = \left(\frac{\sigma_{22}}{Y_T}\right)^2 + \left(\frac{\tau_{12}}{S_{12}}\right)^2 \geq 1 \quad (3)$$

$$M_c = \left(\frac{\sigma_{22}}{2S_{23}}\right)^2 + \left[\left(\frac{Y_C}{2S_{23}}\right)^2 - 1\right]\left(\frac{\sigma_{22}}{Y_C}\right) + \left(\frac{\tau_{12}}{S_{12}}\right)^2 \geq 1 \quad (4)$$

where X_T, X_C, Y_T, Y_C, S_{12}, and S_{23} represent longitudinal tensile strength, longitudinal compressive strength, transverse tensile strength, transverse compressive strength, longitudinal shear strength, and transverse shear strength, respectively. Table 2 includes all strength values used in the present study. β is a coefficient that correlates shear stress to fiber tensile damage; β = zero (default) was used in this work, indicating no shear stress contribution to fiber tensile failure. σ_{11}, σ_{22}, and τ_{12} are components of effective stress tensors. Note that the values of any failure index (F_t, F_c, M_t, and M_c) reaching greater than or equal to 1 refer to damage initiation in an element. More details are available in the pioneering work done by Hashin [52]. In this work, an Abaqus built-in 2D Hashin damage initiation model was used to predict in-plane damage in composite foldcore under quasi-static compressive loading. This Hashin damage model has several limitations, including limited to shell elements only, no damage evolution, and unable to predict 3D stress and deformation fields (thus no out-of-plan damage (i.e., delamination) prediction.

Continuum damage mechanics (CDM) provides a solid theoretical platform for predicting damage evolution in laminated composites. CDM is developed based on a continuum stiffness-

degradation method; stiffness degrades with damage evolution. Scalar damage (index) variables, depending on various damage modes (fiber, matrix, and shear failures), are introduced to characterize damage evolution. The stiffness matrix is updated adaptively at each time increment according to damage status. The evolution of damage variables is based on an energy-dissipation theory and is commonly controlled by either a linear or exponential (softening) law. A more detailed description of the damage evolution laws based on effective plastic displacement and fracture energy can be found in [50]. In this work, a linear damage evolution law was incorporated using the fracture energy dissipated during the damage evolution. The fracture energies used in the model are listed in Table 2.

5.3 Baseline Model Development

A preliminary study, which is not included in this work, showed that altering the bend radius (R in Fig. 5) from 0 to 5 mm had an insignificant impact on the predicted FSC's compressive responses, but significantly increased computational time. Thus, the foldcore was modeled with $R = 0$ and consisted of a series of flat plates. Note that, in practice, a zero bending radius is an ideal case, and an actual Miura foldcore is recommended to be manufactured with a non-zero bending radius to avoid potential demolding issues.

Foldcore unit-cell models were developed with compression platens. The foldcore was discretized with an S4R shell element with a size of 1.5 to 5 mm. A mesh sensitivity study was performed to find the appropriate element size offering acceptable accuracy and computation cost, and the results are included in the following section. The compression platens were created using a 4 mm mesh discrete shell. The boundary conditions employed in the FE model were motivated by mechanical testing and similar models developed by Xiang et al. [53]. As shown in Fig. 9, a uniform compressive displacement of 3 mm/min was applied to the reference point of the upper

platen; an encastred boundary (*i.e.*, no displacements and no rotations) was applied to the bottom platen's reference point.

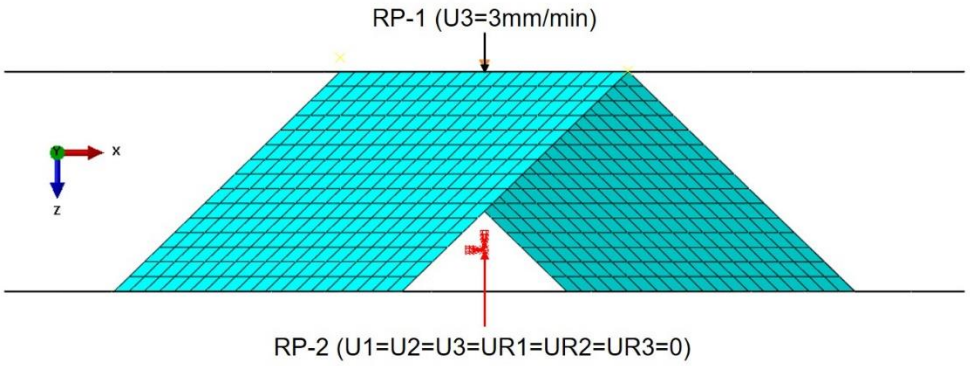

Figure 9. FE model mesh and boundary conditions.

Node-to-surface interactions were applied between the foldcore and compression platens; a node-to-surface interaction was applied to the top crease of the foldcore and the top platen and the bottom crease of the foldcore and the bottom platen. Application of a node-to-surface interaction between the foldcore creases and platens allows to simulate sliding effects as common in mechanical testing. To avoid penetration between the foldcore and platens, nodes-to-surface interaction was applied to the side walls and individual platens. In this work, a friction coefficient of 0.2 and a hard contact were implemented at all contact surfaces.

5.4 Periodic Boundary Condition

Implementation of PBC is critical to approximate a large system by using a small unit-cell. To ensure the appropriate application of PBC, our PBC setup followed the approach introduced by Muhs et al. [54], which utilized a symmetric periodic mesh. Every node along the side walls, except for the bottom nodes and top nodes, is coupled using built-in constraints equations in ABAQUS. Note that the simulation was performed with a single part; no contact types were required. In this work, the PBC was implemented using a linear homogeneous constraint equation in ABAQUS [50,55],

$$A_1 u_i^P + A_2 u_j^Q + \cdots + A_N u_k^R = 0 \quad (5)$$

where P is the node along the side wall, i refers to the degree of freedom (*i.e.,* x-, y-, and z-directions), and A_N is a constant coefficient defining the relative motion of nodes. In this work, PBC was applied to the side edges of foldcore unit-cells.

6 Results and Discussion

6.1 Mesh Sensitivity Study

FE models of foldcore unit-cell specimens were developed using ABAQUS 2021 [50]. Figure 10 compares compressive displacement contours and maximum displacement values, along with computational time for each element size varying from 5 mm to 1.5 mm. As shown in the figure, mesh sizes smaller than 2 mm resulted in a maximum displacement difference of 0.06 mm. The mesh sizes smaller than 1.5 mm showed a negligible variation in the maximum displacement, accompanied by a substantial increase in computational time. Therefore, in this work, the three foldcore unit-cell FE models were discretized using S4R shell elements with an element size of 1.5 mm, yielding 1×1, 1×2, and 2×1 foldcore unit-cell FE models meshed with 1140, 2280, and 2280 elements, respectively.

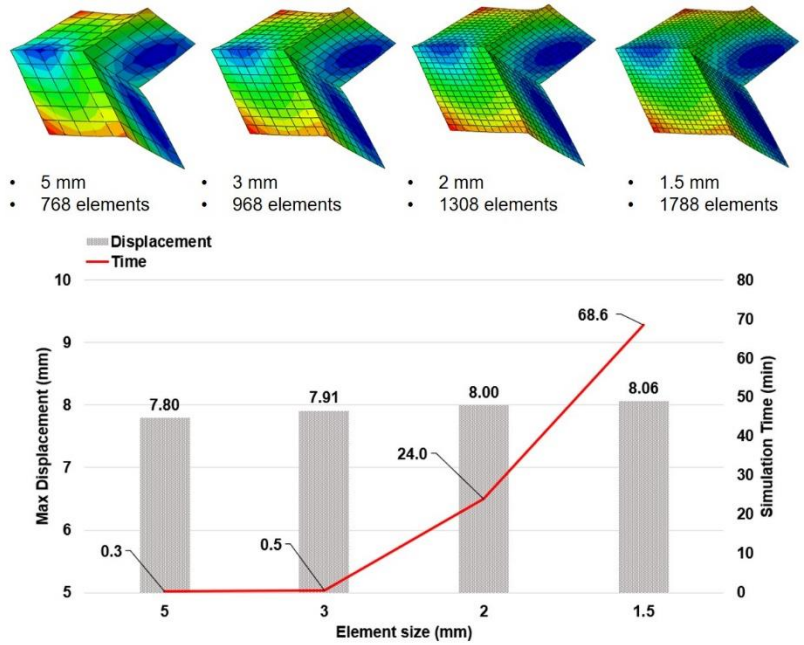

Figure 10. Mesh sensitivity study results.

6.2 Load-Displacement Responses

The compressive load-displacement curves of 1×1, 1×2, and 2×1 foldcore unit-cells obtained from mechanical testing and numerical predictions are compared in Figs. 11a-11c, respectively. In the figure, a range of uncertainty determined from a minimum of four experiments for each unit-cell model is shown by the gray shaded area; average (experimental) load-displacement responses are indicated by the red line, while predicted results, evaluated at the reference point of the top compression platen, are plotted by the blue line. The FE model prediction showed good agreement with the experimental results.

Alternatively, specific energy absorption (SEA) was determined for each unit-cell size by calculating the load-displacement curve according to Eqn. 6:

$$SEA = \frac{E_{abs}}{m_{cr}} = \frac{\int_0^{\delta} F(\delta) d\delta}{m_{cr}} \tag{6}$$

where E_{abs} is the energy absorbed and calculated by integrating the load (F)-displacement (δ) curve. The values obtained from tests and FE simulations were 7.42 kJ and 7.26 kJ (1×1 foldcore),

23.59 kJ and 18.47 kJ (1×2 foldcore), 17.98 kJ and 15.89 kJ (2×1 foldcore), respectively. m_{cr} is the mass of the initial (undamaged) unit-cells. The mass of each unit-cell model is either measured from an actual specimen or estimated from an FE model. For instance, the measured and estimated initial foldcore masses were 4.61 g and 5.72 g (1×1 foldcore), 9.67 g and 10.07g (1×2 foldcore), and 9.43 g and 10.07g (2×1 foldcore), respectively. Overall, the measured and predicted SEA values were comparable, as shown in Fig. 11d. Small differences between the test results and model prediction are primarily associated with complex damage evolution that can be reduced by incorporating relevant damage initiation and evolution laws in the FE model.

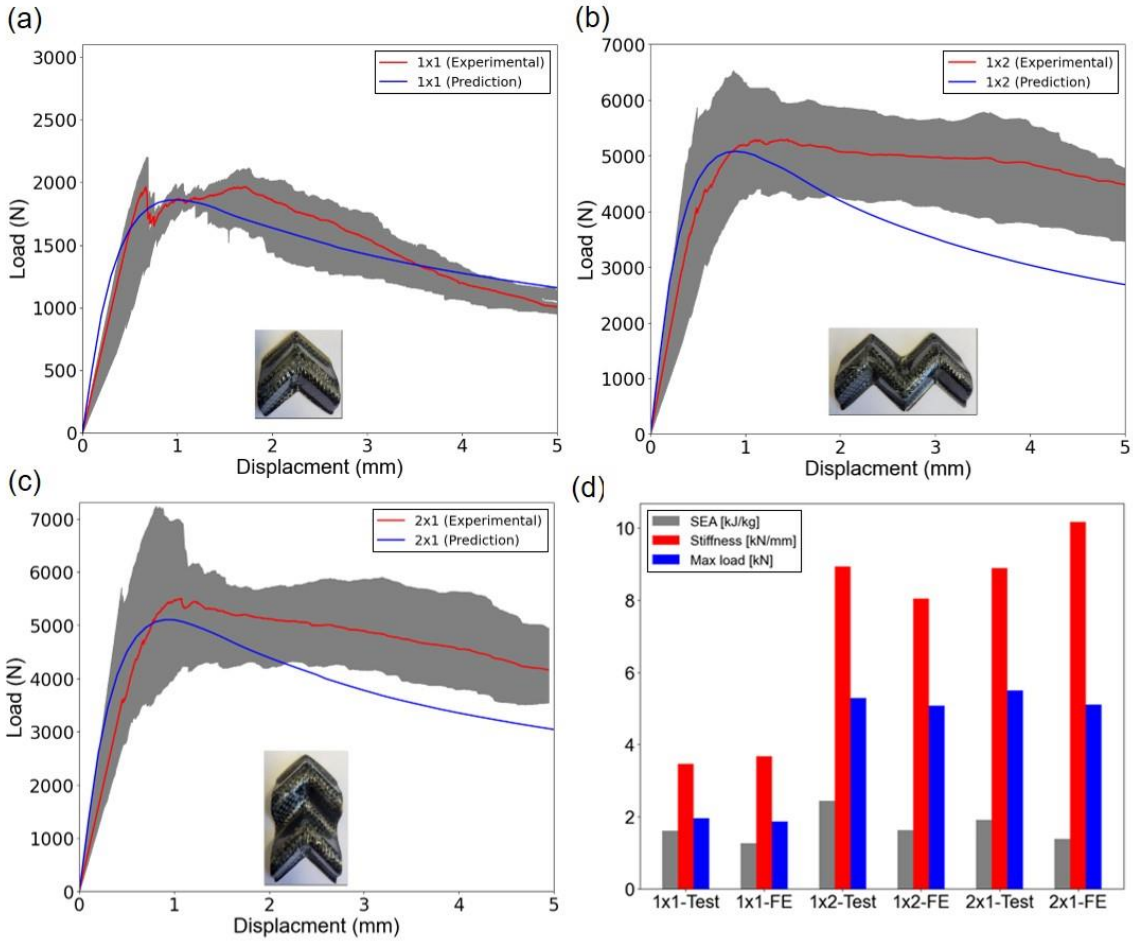

Figure 11. Comparison of measured and predicted load-displacement curves: (a) 1×1, (b) 1×2, (c) 2×1 foldcore unit-cells and (d) bar graphs comparing SEA, max load, and stiffness for all unit-cell sizes and cases.

The FE model prediction showed a < 7% variation in the maximum compressive load and a < 12% variation in compressive stiffness (*i.e.*, slope of a load-displacement curve), compared to the experimental results. In general, the model prediction showed a small underprediction of the maximum compressive load and an overprediction of the compressive stiffness. These are primarily due to (1) non-uniform foldcore dimensions and (2) foldcore specimen sliding observed in mechanical testing. Regardless of size, the foldcore specimens manufactured in this study showed less than approximately 2 mm variations in core thickness t and height H. In fact, carbon/epoxy foldcore is stiff and has complex geometry (*i.e.*, convex top/peak and concave low/valley regions) that requires an aggressive manufacturing process to achieve uniform dimensions across the entire specimen. In our compression tests, a small degree of foldcore specimen sliding was observed during compressive tests due to smooth specimen/platen interactions, causing variations between measured and predicted compressive responses. Such specimen sliding can be avoided by using hydraulic grips or applying a small preload. Although not included in this work, a parametric FE study was performed to understand the effects of various foldcore geometries (thickness, height) and boundary conditions on compressive responses and failure of composite foldcores. The results showed that FE model prediction was *highly* sensitive to foldcore geometric parameters (particularly for thickness) and boundary conditions (where the bottom edges of the core are fixed or simply supported). The accuracy of the current foldcore FE models can be further improved by implementing non-uniform geometric variations (*i.e.*, node shaking, pre-buckling, and varying height [21,56]) and manufacturing imperfections (*i.e.*, defects).

6.3 In-plane Stress and Damage Contours

The von Mises (VM) stress is an excellent stress-based failure criteria developed for a ductile material at the onset of yielding. Many studies showed VM stress contour to show the distribution

and magnitude of stress in composite materials, not for failure prediction; these studies still used conventional composite failure criteria, including Tsai-Wu, Tsai-Hill, Hashin, Puck, Hoffman, and quadric surfaces failure criteria. Two normal stress (σ_{11} and σ_{22}) distribution contours are related due to Poisson's effect, *i.e.*, local stress can be positive in the 1-direction and negative in the 2-direction. Thus, this work include VM stress contours to show the magnitude/severity of stress in foldcore due to quasi-static compressive loading.

Figure. 12 shows the predicted VM stress contour from the representative 1×1 foldcore unit-cell model. The VM stress contour shows that the highest stress levels manifest along the upper region, primarily as a result of the load applied in this specific area. As briefly discussed earlier, foldcore's compressive response strongly depends on fold angle α (Fig. 5). Although not included in this work, it was confirmed that an increase in α results in a decrease in stress concentration at the neighboring wall of the unit-cell creases and a simultaneous increase in the maximum compressive stress values, consistent with [10].

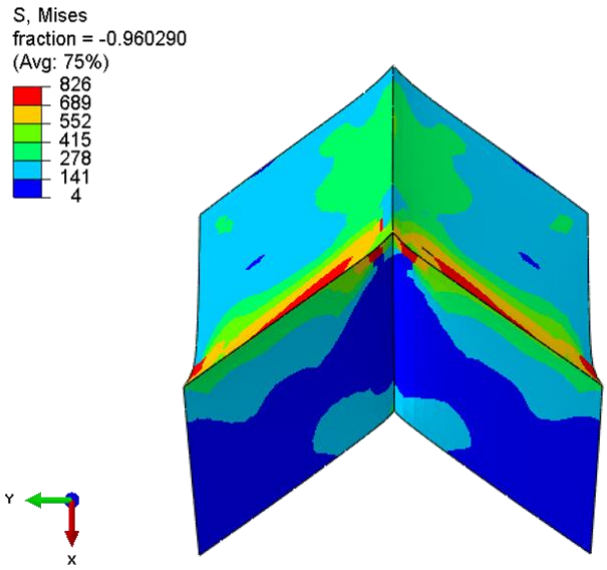

Figure 12. VM stress contour predicted in the 1×1 unit-cell model.

Figures 13a and 13b compare the predicted matrix compressive and tensile failure contours from all subscale foldcore specimens, respectively. When comparing fiber damage with matrix

damage, a larger amount of damage was evident in the matrix; therefore, only the matrix damage contour is displayed. In the figure, red and blue regions indicate complete and no failure. Compression damage in the matrix is predominantly concentrated along the top of the foldcore and the back crease. The damage along the top crease primarily results from the influence of the compression platens, while the damage observed along the back crease is attributed to the foldcore's tendency to flatten out, causing the back crease to fold outward and placing the back into compression. In contrast to the back face, the front crease – a crease located at the bottom center of the foldcore in Fig. 13b – is created by a valley fold resulting from inward folding. As the front crease is subjected to compression, the valley folds outward, resulting in matrix tension damage solely along the front crease. Note that the 2D Hashin damage criteria provide in-plane damage initiation only, so out-of-plane damage (i.e., ply-separation or delamination), was not considered in the current work.

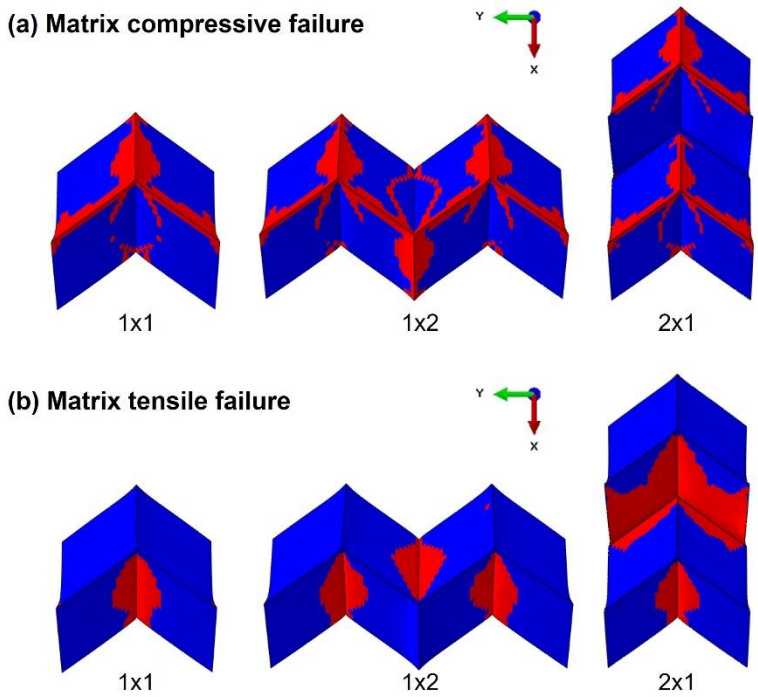

Figure 13. Predicted matrix compressive and tensile failure contours where red and blue regions each indicate failure and no failure.

6.4 Effects of PBC on Compression Responses

Following baseline model analysis with two compression platens, the effects of PBC on subscale foldcore models' compressive responses were investigated. In conventional FE models for various folded-lattice cores with PBC, the bottom edges of the models were fixed with encastred boundary conditions (*i.e.*, no translations and no rotations), and compression platens were not modeled [54]. Thus, the top and bottom compression plates of the baseline FE model (Fig. 9) were removed and encastre boundary conditions were applied to the bottom nodes of each FE model. Furthermore, PBC was implemented at two lateral boundaries (or side creases/edges) of the FE model to eliminate a boundary effect. Similar to the baseline model (Fig. 9), the modified foldcore unit-cell models were discretized with 1.5 mm S4R shell elements. Figure 14 shows the FE models with new boundary conditions used in the following analyses.

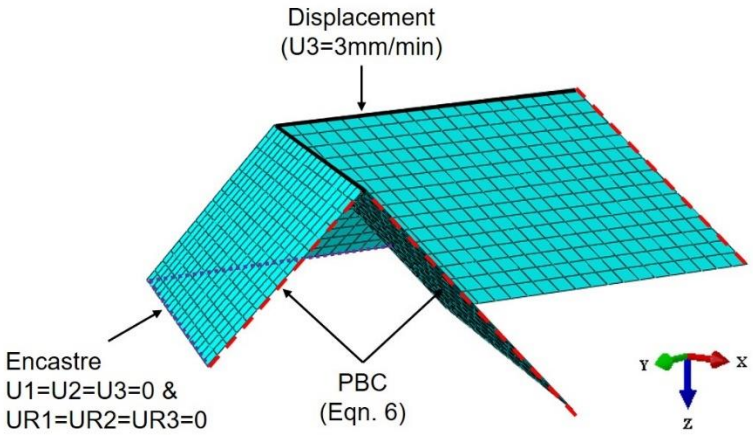

Figure 14. FE model with new boundary conditions.

The predicted VM stress contours obtained from 1×1 unit-cell models with and without PBC are compared in Fig. 15. In the unit-cell model with PBC (Fig. 15a), the nodes along the side walls are symmetric and periodic in accordance with the constraint equation (Eqn. 6), allowing for identical deformation along the side walls. In contrast, the unit-cell model without PBC (Fig. 15b) has the side walls free to move, causing small local buckling near the top and bottom creases of

the unit-cell, but the deformation along the side walls is symmetric, similar to one with PBC (Fig. 15a). Comparing the VM stress contours, the implementation of PBC on a foldcore unit-cell model can avoid edge effects, including local buckling along the side walls.

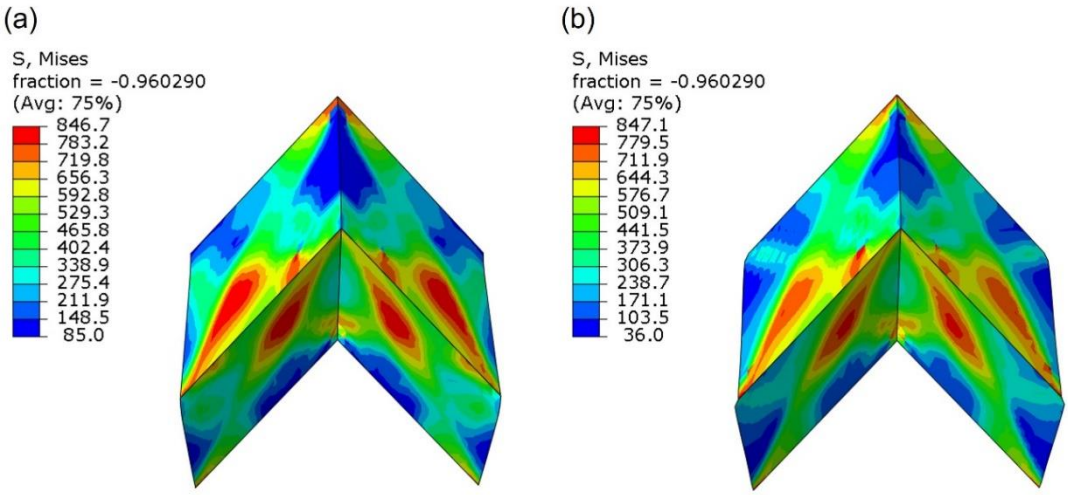

Figure 15. Predicted VM stress contours on a 1×1 foldcore unit-cell model: (a) with PBC and (b) without PBC.

The effects of PBC on a larger unit-cell model were examined to better understand edge effects and sensitivity to a geometric size. The compressive load-displacement curves of various foldcore unit-cell models predicted at the center node of the top crease (Fig. 16a) and the average nodes along the top crease (Fig. 16b) of each unit-cell model were compared. Regardless of PBC implementation, all unit-cell models showed comparable compressive stiffness with an average of 9210 ~ 9212 from the center node (Fig. 16a) and 3150 ~ 3198 from the average of all top nodes (Fig. 16b). The effect of PBC on the load-displacement curve was somewhat negligible in the plastic deformation regime. At the center node of the top crease (Fig. 16a), the predicted maximum compressive load varied from 2739 to 2786 N. This makes sense since a larger unit-cell model provides more structural rigidity and resistance to compressive loading, resulting in a smaller maximum compressive load capacity at the center node. Similarly, the size effect was not significant for both average compressive force and maximum compressive load along the top

nodes (Fig. 16b). The predicted maximum compressive load varies from 804 to 889 N. In this case, the unit-cell models without PBC showed negligible variations in the maximum compressive loads compared to those with PBC. Table 3 summarizes the predicted stiffness and maximum failure loads obtained from all subscale unit-cell models.

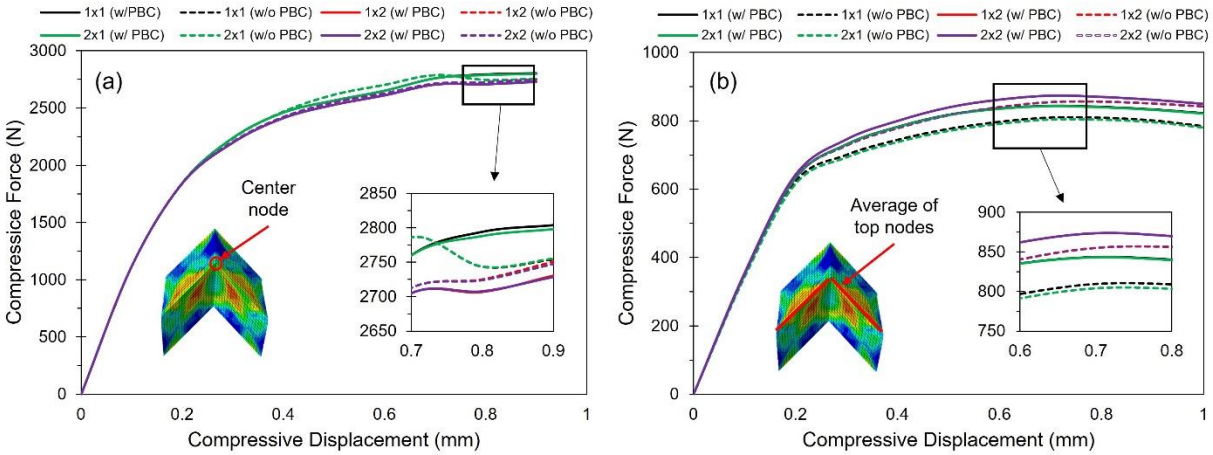

Figure 16. Predicted compressive load-displacement curves of various foldcore unit-cell models calculated at (a) the center node of crease and (b) the top nodes along the top crease.

Table 3. Predicted compressive stiffness and maximum loads from foldcore unit-cell models.

Model	Center node				Average of all top nodes			
	Compressive Stiffness (N/mm)		Max. Compressive Force (N)		Compressive Stiffness (N/mm)		Max. Compressive Force (N)	
	w/ PBC	w/o PBC	w/ PBC	w/o PBC	w/ PBC	w/o PBC	w/ PBC	w/o PBC
1×1	9,217	9,223	2,803	2,786	3,164	3,118	843	809
1×2	9,206	9,215	2,730	2,750	3,213	3,170	874	856
1×4	9,206	9,192	2,739	2,739	3,238	3,215	889	878
2×1	9,223	9,206	2,786	2,751	3,164	3,078	843	804
2×2	9,206	9,215	2,728	2,747	3,213	3,171	874	856
μ	9,212	9,210	2,757	2,755	3,198	3,150	865	841
σ	7	11	31	16	30	47	18	29
CV*	0.08%	0.14%	1.12%	0.58%	0.94%	1.49%	2.08%	3.45%

*Coefficient of variation defined as the ratio of the standard deviation σ to the mean μ.

The compressive stress-strain curves (Fig. 17) exhibited similar characteristics to the load-displacement curves (Fig. 16). In both cases, there was a slight variation when analyzing the center

region, regardless of the presence of PBC. However, a slightly higher deviation was predicted when calculating the average values across the top nodes/elements of the foldcore. In contrast to compressive force-displacement curves (Fig. 16a), the predicted compress stress (Fig. 17a,) did not gradually increase within the plastic regime (after 1% compressive strain). This discrepancy arises because the compressive stress values were derived from four central elements, rather than from a center node. Predicted compressive moduli and strengths were comparable for all unit-cell models, regardless of PBC and subscale model size. In the plastic regime, however, there was a smaller variation (< 2%) in compressive strength. The compressive properties calculated from various foldcore unit-cell models are summarized in Table 4 for reference purposes.

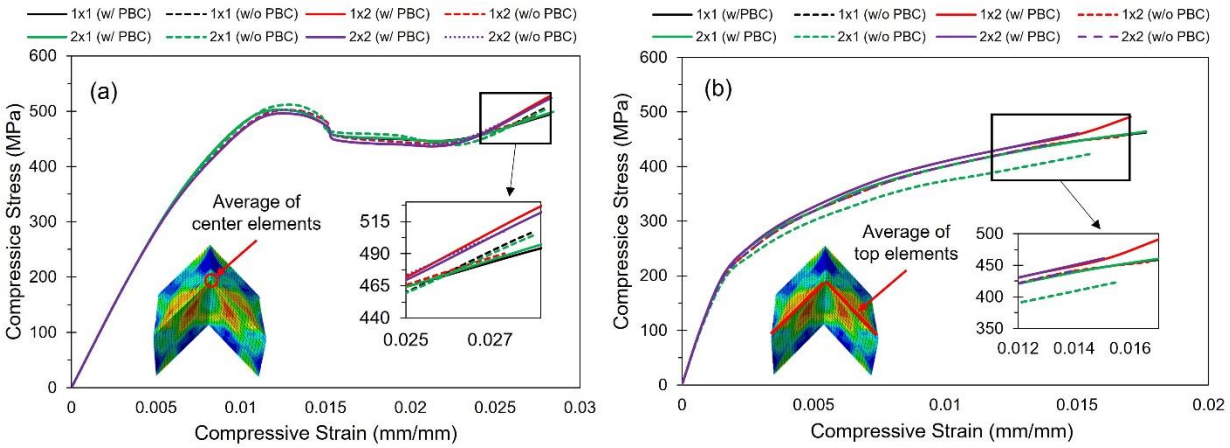

Figure 17. Predicted compressive stress-strain curves of various foldcore unit-cell models at (a) the center elements of top crease and (b) the top elements along the top crease.

Table 4. Predicted compressive moduli and strengths from foldcore unit-cell models.

Model	Average of center elements				Average of all top elements			
	Compressive Modulus (MPa)		Compressive Strength (MPa)		Compressive Modulus (MPa)		Compressive Strength (MPa)	
	w/ PBC	w/o PBC	w/ PBC	w/o PBC	w/ PBC	w/o PBC	w/ PBC	w/o PBC
1×1	59,219	59,176	500	512	143,690	139,001	462	422
1×2	59,245	59,221	528	501	144,701	142,321	491	455
1×4	59,245	59,221	516	517	145,211	144,013	466	458
2×1	59,219	59,176	500	512	143,689	139,001	464	422
2×2	59,245	59,221	524	508	144,701	142,322	461	442
μ	59,234	59,203	514	510	144,674	141,398	469	440

σ	13	22	11	5	608	2,001	11	15
CV*	0.02%	0.04%	2.14%	0.98%	0.42%	1.42%	2.35%	3.41%

*Coefficient of variation defined as the ratio of the standard deviation σ to the mean μ.

As shown in Tables 3 and 4, all foldcore unit-cell models show comparable compressive stiffness, maximum loads, moduli, and strengths, regardless of PBC implementation and subscale size; all coefficient of variation (CV) values were < 3%. Considering the high computational cost of PBC implementation from larger subscale models, PBC is not recommended for subscale foldcore analyses. Small variations in predicted compressive properties likely result from geometric constraints associated with a subscale model size. More details on geometric constraints are discussed in the following sections.

6.5 Periodic Pattern Sequence

As shown in Figs. 16 and 17, the maximum compressive loads and compressive strengths predicted at the center node/elements of the top crease were comparable, but those predicted from the average of the top nodes/elements along the top crease were relatively varied. This suggests that the model's accuracy may depend on the periodic placement of unit-cells. It is expected that unit-cells placed in *parallel* (or in a row-wise direction) interact differently with those placed in *perpendicular* (or in a column-wise direction). Hence, we further investigated the influence of periodic unit-cell placement on the compressive responses of various subscale foldcore models.

Figure 18 compares the predicted VM stress contours of two 1×1 foldcore unit-cell models mirrored about the x-z plane (indicated by red dotted lines) and two 1×2 foldcore unit-cell models with and without PBC. Overall, each unit-cell model showed comparable VM stress contour. Predicted VM stresses were slightly different at the edges shared with two neighboring foldcore unit-cells. A small variation in VM stress distribution results from local buckling occurring in the

middle of the shared edge during compression. For instance, two lateral edges of a 1×1 foldcore unit-cell can be buckled, regardless of PBC, by a downward compression force. The region with local buckling (blue) is noticeable in the mirrored foldcore models (Figs. 18a and 18c). However, local buckling was not predicted in 1×2 foldcore unit-cell models (Figs. 18b and 18d) due to resistance associated with geometric constraint of individual foldcores. All four 1×2 unit-cell models shown in Fig. 18 predicted similar VM stress distributions, although small differences can be found near the shared edge. This suggests that a 1×1 unit-cell model without PBC is sufficient to predict the quasi-static compressive response of foldcore composite.

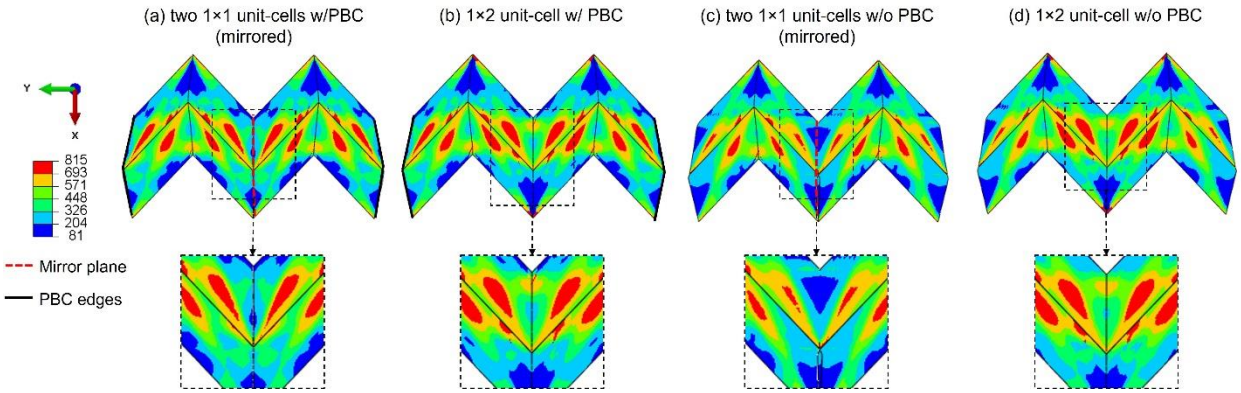

Figure 18. VM stress contours of 1×2 foldcore unit-cell models with and without PBC.

In contrast, there was no interaction between two 1×1 unit-cells when they were placed *perpendicular* to each other, as shown in Fig. 19. Regardless of the implementation of mirroring and PBC techniques, all four 2×1 unit-cell models predicted nearly identical VM stress distributions. This is expected since the bottom creases of foldcore unit-cell are encastred. This finding also suggests that the implementation of PBC on a foldcore unit-cell model is not essential to capture an accurate structure response to quasi-static compressive loading.

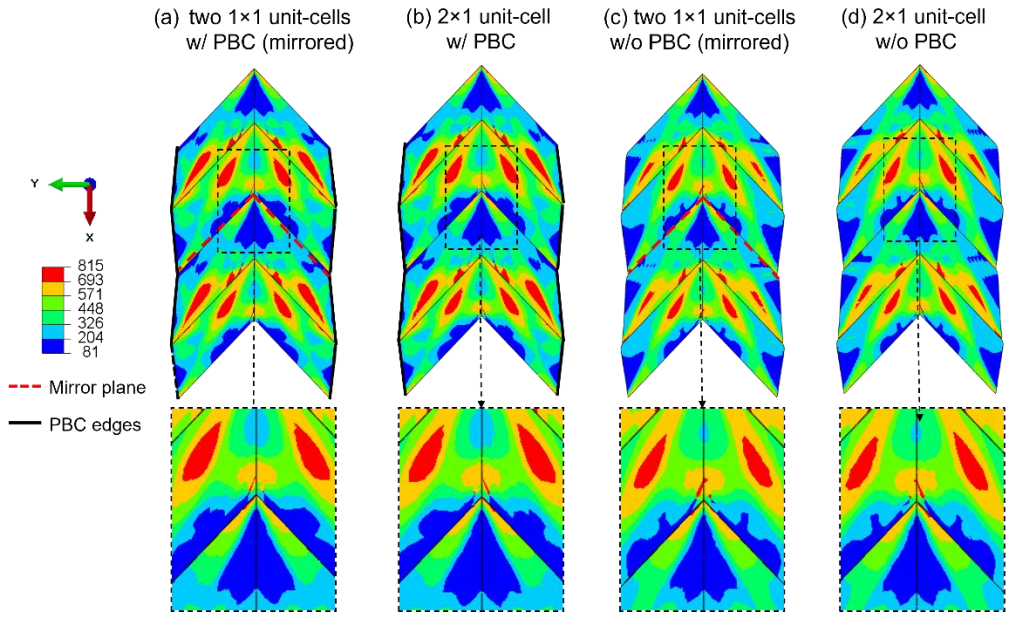

Figure 19. VM stress contours of 2×1 foldcore unit-cell models with and without PBC.

7 Conclusion

The quasi-static compressive responses of various subscale carbon fiber-reinforced epoxy Miura foldcores were investigated through a combination of mechanical tests and ABAQUS finite element (FE) simulations. Representative volume element (RVE) models for three subscale foldcore models were developed with periodic boundary conditions (PBC) using homogenized composite properties through a two-step homogenization process using NASA's multiscale analysis tool (NASMAT). The FE model prediction showed good agreement with quasi-static compressive test results. The present study concludes:

- The FE models of the three subscale Miura foldcores demonstrated maximum compressive load and compressive stress values that closely matched those obtained from mechanical testing. When compared to mechanical testing results, the 1×1, 1×2, and 2×1 foldcore RVE models each exhibited 5%, 7%, and 11% variations in the compressive stiffness, and 5%,4%, and 7% variations in the peak compressive force.

- Subscale foldcore models incorporating PBC demonstrated <4% variations in predicted compressive properties (stiffness, modulus, maximum stress, and maximum force) compared to those without PBC. These small differences between PBC and non-PBC models were attributed to additional geometric constraints along the side walls of each foldcore unit-cell. However, applying PBC in foldcore RVE models substantially increased computational time by at least 50%. This suggests that implementing PBC for subscale foldcore analysis may not be recommended.
- The investigation of the periodic pattern sequence revealed that, regardless of PBC, foldcore unit-cells placed in parallel and perpendicular exhibited similar overall stress distributions. A small variation in stress distribution, resulting from local buckling in the presence of PBC, was predicted along the center crease, where the two single foldcore unit-cells were connected in parallel. The model suggests that a 1×1 foldcore unit-cell model without PBC is sufficient to predict accurate quasi-static compressive responses of foldcore composite.

An integrated testing and FE modeling framework provides a solid foundation for future investigations on the design of large-scale Miura foldcore composites with highly tailorable material properties. This study primarily focused on core geometric constraints associated with various subscale, neighboring wall interactions, and edge effects. Material selection and associated manufacturing process will be other critical parameters influencing the mechanical properties of foldcore composites. Notably, all Miura foldcores exhibit a complex core geometry compared to that of conventional honeycomb cores. The use of stiffer materials, along with the manufacturing of multi-layered foldcores, requires aggressive manufacturing conditions to preserve precise core geometry. Futhremore, improper manufacturing processes can lead to significant property degradation, resulting from uncontrolled defect generation and distribution. Incorporating

manufacturing-induced defects and other damage initiation and evolution criteria into subscale foldcore analyses has the potential to significantly improve the predictive modeling accuracy of the model. A future investigation will explore various manufacturing-induced defects in foldcore composites and their implementation into subscale analyses.

Acknowledgements

Acknowledgment goes to Nathan Hoch for his initial work on this research.

Declaration of conflicting interests

The author(s) declared no potential conflicts of interest with respect to the research, authorship, and/or publication of this article.

Funding

The author(s) disclosed receipt of the following financial support for the research, authorship, and/or publication of this article: This work was supported by the 2023 Hanwha Non-Tenured Faculty Award; USU CoE Undergraduate Research Program (EURP) fellowship.

References

[1] Bitzer TN. Honeycomb Technology: Materials, Design, Manufacturing, Applications and Testing - T.N. Bitzer - Google Books. First, Chapman & Hall; 1997, p. 3–20.
[2] Olympio KR, Gandhi F. Flexible skins for morphing aircraft using cellular honeycomb cores. J Intell Mater Syst Struct 2010;21:1719–35.
[3] Koryo M. Zeta-Core Sandwich - Its Concept and Realization. vol. 37. 1972.
[4] Rastogi M. Moisutre Ingress in Honeycomb Sandwich Composite Structures-Effects & Detection. IJERT 2016;5:171–6.
[5] Miura K. New structural form of sandwich core. J Aircr 1975;12:437–41.
[6] Fischer S, Drechsler K, Kilchert S, Johnson A. Mechanical tests for foldcore base material properties. Compos Part A Appl Sci Manuf 2009;40:1941–52.
[7] Khaliulin VI, Inkin VA. Calculation of process variables at composite Z-crimp shaping using the folding method. Russian Aeronautics (Iz VUZ) 2013;55:417–23.
[8] Johnson AF. Novel Hybrid Structural Core Sandwich Materials for Aircraft Applications. 11th Euro-Japanese Symposium on Composite Materials 2008.
[9] Fan H-L, Zeng T, Fang D-N, Yang W, Fan H, Zeng T, et al. Mechanics of advanced fiber reinforced lattice composites. Acta Mechanica Sinica 2011;26:825–35.
[10] Heimbs S, Cichosz J, Klaus M, Kilchert S, Johnson AF. Sandwich structures with textile-reinforced composite foldcores under impact loads. Compos Struct 2010;92:1485–97.

[11] Grzeschik M. Performance of Foldcores Mechanical Properties and Testing. Proceedings of the ASME Design Engineering Technical Conference 2014;6 B.
[12] Oei M, Klett Y, Harder N, Flemming D, Sawodny O. Modelling the Flow and Heat Transfer Characteristics of Perforated Foldcore Sandwich Composites for Application in Room Air Conditioning. IEEE International Conference on Automation Science and Engineering 2019;2019-August:1269–74.
[13] Heimbs S, Middendorf P, Kilchert S, Johnson AF, Maier M. Experimental and numerical analysis of composite folded sandwich core structures under compression. Applied Composite Materials 2007;14:363–77.
[14] Klett Y, Drechsler K, Wang-Iverson P, Lang RJ, Yim M. Designing technical tessellations. Origami 5: Fifth International Meeting of Origami Science, Mathematics, and Education 2011:305–22.
[15] Chen Y, Zeng X, Deng Y, Wei G. Investigation on Manufacturing and Low-Velocity Impact Performance of All-Composite Sandwich Structure with S-Type Foldcore. Compos Struct 2022;290:115539.
[16] Gattas JM, You Z. The behaviour of curved-crease foldcores under low-velocity impact loads. Int J Solids Struct 2015;53:80–91.
[17] Cheng J, Li Y. Foldcore Structures with Origami Initiators for Energy-Absorbing Sandwich Panels. Acta Mechanica Solida Sinica 2023;36:491–505.
[18] Xiang XM, Lu G, You Z. Energy Absorption of Origami Inspired Structures and Materials. Thin-Walled Structures 2020;157:107130.
[19] Heimbs S, Kilchert S, Fischer S, Klausrwth M, Baranger E. Sandwich Structures with Folded Core: Mechanical Modeling and Impact Simulations. Proceeding of SAMPE Europe International Conference (SEICO-09), Paris, France: 2009.
[20] Muhs F, Thissen S, Middendorf P. Virtual process chain for optimization of sandwich foldcores under flatwise compression. Thin-Walled Structures 2020;157:107121.
[21] Heimbs S, Middendorf P, Kilchert S, Johnson AF, Maier M. Numerical Simulation of Advanced Folded Core Materials for Structural Sandwich Applications. 1st CEAS European Air and Space Conference, 2007, p. 2889–95.
[22] Zhou X, Wang H, You Z. Mechanical Properties of Miura-Based Folded Cores under Quasi-Static Loads. Thin-Walled Structures 2014;82:296–310.
[23] Xiang XM, You Z, Lu G. Rectangular Sandwich Plates with Miura-Ori Folded Core Under Quasi-Static Loadings. Compos Struct 2018;195:359–74.
[24] Wang M, Karagiozova D, Lu G. Quasi-Static Three-Point Bending of Sandwich Panels with Miura-Ori Cores. Int J Mech Sci 2024;268:109010.
[25] Yuping E, Yang G, Zhu X, Lu G, Sun J. Experimental Study on the Flat-Wise Compression of Foldcore Sandwich Paperboard. Thin-Walled Structures 2022;181:110017.
[26] Zhou C, Liu W, Ge C, Song Z, Du K, Wang B. Energy Absorption of a Novel Dual-Defect Miura Foldcore Subject to Quasi-Static Axial Crushing. Materials Engineering 2023.
[27] Kankkunen T, Niiranen J, Kouko J, Palmu M, Peltonen K. Parametric Linear Finite Element Stress and Stability Analysis of Isotropic and Orthotropic Self-Supporting Miura-Ori Structures. Mechanics of Advanced Materials and Structures 2022;29:5808–22.
[28] Lv Y, Zhang Y, Gong N, Li Z xian, Lu G, Xiang X. On the Out-Of-Plane Compression of A Miura-Ori Patterned Sheet. Int J Mech Sci 2019;161–162:105022.
[29] Gattas JM, You Z. Quasi-Static Impact Response of Alternative Origami-Core Sandwich Panels. Proceedings of the ASME Design Engineering Technical Conference 2014;6 B.

[30] Heimbs S. Foldcore Sandwich Structures and Their Impact Behaviour: An Overview. Solid Mechanics and Its Applications 2013;192:491–544. https://doi.org/10.1007/978-94-007-5329-7_11.
[31] Du Y, Song C, Xiong J, Wu L. Fabrication and Mechanical Behaviors of Carbon Fiber Reinforced Composite Foldcore Based on Curved-Crease Origami. Compos Sci Technol 2019;174:94–105.
[32] Karagiozova D, Wang M, Lu G. The Compressive and Shear Characteristics of Miura-ori Forms as Core Materials of Sandwich Structures. Acta Mechanica Solida Sinica 2023;36:531–40.
[33] Kankkunen T, Niiranen J, Kouko J, Palmu M, Peltonen K. Parametric Linear Finite Element Stress and Stability Analysis of Isotropic and Orthotropic Self-Supporting Miura-Ori Structures. Mechanics of Advanced Materials and Structures 2022;29:5808–22.
[34] Ma J, Dai H, Chai S, Chen Y. Energy Absorption of Sandwich Structures with a Kirigami-Inspired Pyramid Foldcore under Quasi-Static Compression and Shear. Mater Des 2021;206:109808.
[35] Hao Y, Zang S, Wang H, You Z, Zhou X. Virtual Testing of Foldcores made of Polyethylene Terephthalate. 20th International Conference on Composite Materials, Copenhagen, Denmark: 2015.
[36] Huang K, Song K, Zhou X, Ji B, Wang H. Quasi-Static Mechanical Properties of Composite Foldcores based on the BCH Patterns. Thin-Walled Structures 2022;171:108776.
[37] Xiang XM, Lu G, You Z. Energy Absorption of Origami Inspired Structures and Materials. Thin-Walled Structures 2020;157:107130.
[38] Deng A, Ji B, Zhou X, You Z. Geometric Design and Mechanical Properties of Foldcores Based on the Generalized Resch Patterns. Thin-Walled Structures 2020;148:106516.
[39] Gattas JM, You Z. The Behaviour of Curved-Crease Foldcores under Low-Velocity Impact Loads. Int J Solids Struct 2015;53:80–91.
[40] Heimbs S, Cichosz J, Kilchert S, Klaus M. Sandwich Panels with Cellular Cores Made of Folded Composite Material: Mechanical Behaviour and Impact Performance. 17th International Conference on Composite Materials (ICCM-17), Edinburgh, UK: 2009.
[41] Hexcel Corporation. HexPly ® 3501-6 2014.
[42] Hoch N, Mortensen C, Lee J, Harrison K, Kota KR, Lacy T. Hyper-Velocity Impact Performance of Foldcore Sandwich Composites. Proceedings of the 37th American Society for Composites (ASC) Technical Conference, Tucson, AZ: 2022.
[43] Mortensen C, Hoch N, Lee J. Directionally Controlled Impact-Debris Propagation of Origami-Inspired Composite Panels . 2022 ASME International Mechanical Engineering Congress & Exposition (IMECE), Columbus, OH: 2022 ASME International Mechanical Engineering Congress & Exposition (IMECE); 2022.
[44] Hoch N, Mortensen C, Lee J, Harrison K, Kota K, Lacy T. Hyper-Velocity Impact Performance of Foldcore Sandwich Composites. 37th American Society for Composites (ASC) Technical Conference, Tucson: 2022.
[45] ASTM:D695. Standard Test Method for Compressive Properties of Rigid Plastics 1. ASTM International 2015.
[46] Hearley B. Multiscale Modeling of Unreinforced Textile Fabrics in Nasmat. North Carolina State University; 2021.
[47] Augl JM. Moisture Effects on the Mechanical Properties of Hercules 3501–6 Epoxy Resin. Silver Spring, MD: 1979.

[48] Liu K. Micromechanics based Multiscale Modeling of the Inelastic Response and Failure of Complex Architecture Composites. Arizona State University; 2011.
[49] Haldar S, Lopes CS, Gonzalez C. Interlaminar and Intralaminar Fracture Behavior of Carbon Fiber Reinforced Polymer Composites. Key Eng Mater 2016;713:325–8.
[50] Dassault Systèmes Simulia. ABAQUS 2021 Documentation. 2022.
[51] Pham DC, Cui X, Ren X, Lua J. A Discrete Crack Informed 3D Continuum Damage Model and Its Application for Delamination Migration in Composite Laminates. Compos B Eng 2019;165:554–62.
[52] Hashin Z. Failure Criteria for Unidirectional Fiber Composites. J Appl Mech 1980;47:329–34.
[53] Xiang X, Shao D, Zhang X, Sharif U, Ha NS, Xiang L, et al. Sandwich Structures with Tapered Tubes as Core: A Quasi-Static Investigation. Defence Technology 2023.
[54] Muhs F, Thissen S, Middendorf P. Virtual Process Chain for Optimization of Sandwich Foldcores under Flatwise Compression. Thin-Walled Structures 2020;157:107121.
[55] Wu W, Owino J, Al-Ostaz A, Cai L. Applying Periodic Boundary Conditions in Finite Element Analysis. SIMULIA Community Conference, 2014, p. 707–19.
[56] Fischer S. Realistic FE simulation of foldcore sandwich structures. International Journal of Mechanical and Materials Engineering 2015;10:1–11.